Fig 5

Dynamic localization of recombination factors during mutant meiosis. (A) Top left: Schematic depicting the positions of nuclei just prior to the early-to-late prophase transition (*), which is delayed in mutants deficient in crossing over. Top right: Quantification of RPA-1 and RAD-51 foci in nuclei from the positions indicated in the schematic; foci levels for all mutants are significantly higher than WT ($p < 0.0001$). Bottom: Representative examples of such nuclei. **(B)** Early-to-late prophase transition region of WT (top) and *cosa-1* mutant (bottom) gonad, stained for MSH-5, HTP-3 and early prophase marker DSB-1. MSH-5 foci are not retained after the transition to late prophase in the *cosa-1* mutant (see also Fig S4B). **(C)** Early prophase (red outline), early-to-late prophase transition (yellow) and late prophase (green) nuclei from a *syp-1* mutant gonad. Throughout the prolonged early prophase of *syp-1* mutants, MSH-5 colocalizes with BLM foci (left). At the transition to late prophase, MSH-5 foci reduce in number, and BLM is still present (middle). Upon transition to late prophase, BLM is lost from MSH-5-marked sites (right). Scale bar: 5 µm. **(D)** Left: late prophase nuclei from WT (*gfp::cosa-1*) and the *syp-3* mutant (*syp-3; gfp::cosa-1*). Right: Quantification of late prophase MSH-5/COSA-1 foci. **(E)** Representative SIM images of early prophase (red outline), early-to-late-prophase transition (yellow) and late prophase (green) nuclei from *syp-1*; *blm::HA* worms (scale bar: 1 µm; with enlarged individually cropped DNA repair sites from the same fields shown below (scale bar: 500 nm). In late prophase nuclei of the *syp-1* mutant, MSH-5 doublets are association with and oriented along single unpaired axes without BLM being present, as indicated in the schematic.

Supplemental Information:

Supplemental Figure Legends:

Fig S1 Improved visualization and dynamic localization of DNA repair complexes during meiotic prophase progression (related to Figure 1).

(A) Nuclear lysis and chromosome spreading improve visualization of DNA repair complexes at sites of ongoing meiotic recombination. Example images of zygotene/early pachytene nuclei prepared using either a whole mount *in situ* method (according to: (Jagut et al., 2016); left panel) or detergent-based nuclear lysis and chromosome spreading procedure (according to: (Pattabiraman et al., 2017); right panel), probed for: BLM, a DNA helicase [HIM-6 tagged by HA (*him-6::HA*), expressed from the endogenous locus; green], MSH-5, a pro-crossover factor (red) and HTP-3, a core component of the meiotic chromosome axis (grey). Wide-field microscopy with subsequent 3D-deconvolution and Z-stack projection is indicated as “WF”; scale bars represent 5 μm. **(B) Appearance, disappearance and localization of RAD-51 and RPA-1 and over the course of meiotic prophase.** Spread WT gonad probed for RAD-51 (red), RPA-1 (green), DSB-2 (marker of early prophase; purple) and HTP-3 (grey in the top panel and blue in the middle panel). Meiotic prophase progresses from left (leptotene) to right (diplotene). Boxes represent the enlarged fields displayed in Fig 1A. Scale bar represents 5 μm. **(C-D) MSH-5 marks inter-homolog DNA repair events. (C)** Left: Schematics of pachytene chromosome arrangement in WT and in *zim-2* mutants, which are specifically defective for pairing and synapsis of chromosome V (cyan). Right: SIM images of spread nuclei from *zim-2* gonads at the early-to-late prophase transition, probed for: MSH-5 (yellow), SYP-1 (blue) and HTP-3 (red, if localizing with SYP-1, and pseudo-colored cyan when unsynapsed, indicating the unpaired Chr. V). MSH-5 foci are found on all synapsed chromosome pairs but not on the two unsynapsed chromosomes. Scale bar represents 1 μm. **(D)** Left: Schematics comparing WT chromosome II synapsis configuration with the chromosome II synapsis configuration in worms heterozygous for *mIn1*, which carries a large internal inversion and an integrated high-copy transgene array (indicated in green). Right: wide-field images of spread nuclei from gonads of *mIn1/+* animals, probed for RAD-51 (magenta), MSH-5 (green), HTP-3 (red) and SYP-1 (blue). MSH-5 foci are absent from the chromosomes segments that are enriched for RAD-51-marked intermediates, which are presumed to correspond to heterosynapsed chromosome segments where inter-homolog recombination intermediates cannot form; these segments are pseudo-colored in purple in the left panels. Scale bars represent 5 μm.

Fig S2 Dynamic localization of BLM, MSH-5, COSA-1 and RPA-1 during meiotic prophase (related to Figure 1)**.**

(A) Spread gonad, probed for BLM (HIM-6::HA, red), MSH-5 (green), GFP::COSA-1 (blue), and HTP-3 (grey). COSA-1 is tagged with GFP (*gfp::cosa-1*) and expressed from an randomly integrated overexpression construct in the background of the *cosa-1(tm3298)* deletion. Representative fields of early pachytene, early-to-late pachytene transition and late pachytene demonstrate that all COSA-1 foci localize with MSH-5 foci, and MSH-5 foci nearly always colocalize with BLM foci. BLM, in contrast, can be detected without MSH-5/COSA-1, especially during the early-to-late prophase transition. Please note changes of colors for different markers in the enlargements to visualize co-localization. Scale bars represent 5 μm. The inset graph depicts measurements of the maximum brightness values (sorted from dimmest to brightest) of 20 individual GFP::COSA-1 foci for each of the indicated meiotic prophase stages and at 20 control regions inside and outside of nuclei (background fluorescence levels). Regions of the gonad where measurements were taken are indicated by dashed boxes of corresponding color on the enlarged images. The ranges of maximum brightness intensities for early and late foci did not overlap, indicating that early and late COSA-1 foci can be distinguished as separate classes.

(B) Representative fields of early pachytene, early-to-late pachytene transition and late pachytene nuclei, probed for GFP::COSA-1 (blue), RPA-1 (red), BLM (HIM-6::HA, green) and HTP-3 (grey). During early pachytene, BLM and early (dim) COSA-1 foci strictly colocalize with RPA-1 foci. At the early-to-late pachytene transition, BLM and RPA are frequently found at different sites. In late pachytene and diplotene, BLM foci at designated CO sites, which are co-decorated by a late (bright) COSA-1 focus, are largely free of RPA-1. Scale bars represent 5 μm. **(C)** Graph depicting quantitation of MSH-5, BLM and RPA foci in early pachytene nuclei from the region of the gonad where recombination sites are detected at maximum levels (see STAR Methods). Mean values for individual gonads are plotted separately (20 nuclei score per gonad); error bars indicate standard deviation. One-way ANOVA did not detect significant differences among the means for MSH-5 foci (6 gonads), for BLM foci (3 gonads), or RPA foci (3 gonads). Paired t-testing indicated that numbers of MSH-5 foci and BLM foci within nuclei were strongly correlated (r = 0.798, p <0.0001), and an average of 3.4 ± 2.7 more BLM foci than MSH-5 foci were detected per nucleus (p <0.0001). Numbers of MSH-5 and RPA foci within nuclei were also correlated (r = 0.594, p <0.0001), and an average of 7.5 ± 3.1 more RPA foci than MSH-5 foci were detected per nucleus (p <0.0001).

Fig S3 Validation, measurements and feature quantification for SIM imaging (related to Figures 2 and 3).

(A) Five 100 nm, 4-color beads (”Tetra-Speck beads”) mounted in Vectashield +10% 1xPBS-T (to mimic conditions used for our biological samples) imaged in all four channels using either wide field imaging and deconvolution (top), or SIM and 3D-reconstruction (bottom) prior to maximum-intensity Z-stack-projection. Brightness and contrast were not adjusted post SIM-reconstruction or deconvolution for the display of these images. Actual bead size (100 nm) is depicted on the bottom right in each frame in pseudo-color. All beads in the field of view can be clearly resolved as single, round entities in all four channels using SIM, validating the accuracy of SIM reconstruction. **(B)** Left, graph indicating distances measured between paired BLM foci and paired MSH-5 foci at late pachytene CO-designated sites (as depicted in Figure 3) and distances separating paired chromosome axes (as indicated by HTP-3 immunostaining) measured in different types of cytological preparations. The SC-CR is partially destabilized under the hypotonic spreading conditions (“$H_2 0$”) used here for visualization of recombination site architecture in the context of chromosome axes (Pattabiraman et al., 2017) resulting in a significant increase (up to two-fold) in the separation between homologous chromosome axes in late pachytene nuclei relative to the roughly 120-170 nm distances measured *in situ* (Kohler et al., 2017; Schild-Prufert et al., 2011); this work)). Under the more physiological/hypertonic salt conditions used for visualizing recombination sites in relation to the SC-CR (“Hanks”; see Methods), the SC-CR is more stable, and inter-axis distance measurements are indistinguishable from measurements made using SIM images of SCs in nuclei from whole mount *in situ* preparations. Horizontal lines indicate the mean, error bars indicate standard deviation. Numbers of measurements represented in the graph (n) were as follows: BLM-BLM, n=20; MSH-5-MSH-5, n=19; HTP-3-HTP-3 ($H_2 0$), n=52; HTP-3-HTP-3 (Hanks), n=30; HTP-3-HTP-3 (*in situ*), n=51.

Right, sample SIM images of SCs from a whole-mount *in situ* preparation; scale bar: 1 µm. **(C)** Quantification of MSH-5, BLM and COSA-1 doublet, elongated or singlet foci and orientation with respect to chromosome axes (as depicted in the graphical key below pie charts) at all 150 CO sites in 25 late pachytene nuclei. **(D)** Left: the theoretical angles of a line between the two peaks in a doublet recombination focus relative to the chromosome axes of the SC (depicted in frontal view). Right: overlaid dashed lines indicate actual measurements of angles for late pachytene BLM doublets at CO sites relative to the chromosome axes (n=18). **(E)** Quantification of BLM and MSH-5 singlet and doublet foci (as depicted in the graphical key below) at 120 CO sites in 20 late diplotene nuclei.

Fig S4 SIM imaging of SC-CR organization in relation to recombination sites (related to Figures 4).

(A) Example SIM image of an early pachytene nucleus, probed for the SC-CR protein SYP-1 (red) and BLM (green). In most cases, BLM appears laterally associated with continuous stretches of SC-CR proteins (indicated by green circles). At only few sites, BLM directly co-localizes with the SC-CR-protein (red circles). The scale bar represents 1 µm. **(B)** Examples of computationally straightened late pachytene SCs probed for the N-terminus (red) and C-terminus (green) of SYP-1. SYP-1 forms a continuous stretch along the bivalent, and at only one site per bivalent, a clear SYP-1 bubble is visible. Straightened chromosomes were aligned at the bubble. Right: PLK-2::HA (blue), a Polo-like kinase, localizes from late pachytene onward to the short arm of the bivalent, *i.e.* from the CO site to the nearest chromosome end; PLK-2::HA also forms a focus inside the SC-CR bubble. The scale bar represents 1 µm. **(C)** Field of late pachytene/diplotene nuclei from a *spo-11* gonad, which lacks the enzyme responsible for forming canonical meiotic DSBs, probed for HTP-3 (red), SYP-1 (green) and MSH-5 (blue). Although *spo-11* mutants are unable to generate canonical meiotic DSBs, a subset of nuclei chromosomes (5% at 25˚C) nevertheless acquires a single recombination focus during late prophase, presumably reflecting the occurrence of spontaneous DNA lesions that recruit meiotic DNA repair proteins. The SC-CR proteins become preferentially concentrated specifically on the subset of chromosomes that received a recombination focus (Machovina et al., 2016; Nadarajan et al., 2017; Pattabiraman et al., 2017), and on such chromosomes, the SC-CR becomes prominently enriched around and engulfs these recombination foci. These foci most likely do not mark *bona fide* recombination events, as: 1) These sites do not reliably adopt the complex architecture observed at meiotic recombination sites in the WT; 2) These sites appear in many cases to occur between sister chromatids, accompanied by local alterations in synaptic configuration never seen in the WT (*e.g.* example on the right); crossover recombination is absent in *spo-11* when measured genetically (Dernburg et al., 1998). Scale bars represent 5 μm (large field) and 1 μm (inset). **(D)** Whereas each chromosome pair normally harbors only a single COSA-1-marked CO site, the two-chromosome fusion *mnT12(IV;X)* harbors two widely-spaced COSA-1-marked CO sites in a subset of meioses (Yokoo et al., 2012; Libuda et al., 2013). The SIM image presented here shows an individually cropped *mnT12* bivalent (from the early diplotene nucleus highlighted at the left) with two CO sites, each marked by COSA-1 and MSH-5; both CO sites, are engulfed by the SC-CR (SYP-1), which is strongly enriched around these sites. Scale bar is 2.5 μm.

Fig S5 Localization of Meiotic DNA repair complexes in SC-CR and CO-defective mutants (related to Figure 5).

(A) BLM and RPA-1 colocalize in early prophase in SC-CR- and CO-defective mutants. Representative early prophase nuclei from spread gonads probed for BLM::HA, RPA-1 and HTP-3 from WT, null mutants of *syp-1*, *cosa-1*, and *zhp-3*, and a temperature-sensitive *msh-4* mutant. *msh-4ts; him6::HA* animals were grown at 25˚C and analyzed 16 hours post L4 larval stage; all other genotypes were assessed under standard conditions (20˚C and 24h post L4). Despite higher numbers of recombination foci than in WT, all BLM foci co-localize with RPA-1 foci during early prophase in all these CO-deficient mutants. Please note changes of colors for different markers in the different panels to visualize co-localization. Scale bars represent 5 μm. **(B) DNA repair proteins disappear from chromosomes at the delayed early-to-late prophase transition in a CO-defective mutant.** Images of WT and *zhp-3* mutant germ lines, probed for RAD-51 (red), MSH-5 (green) and HTP-3 (grey), demonstrating the loss of both MSH-5 and RAD-51 foci in the *zhp-3* mutant upon (delayed) transition to late pachytene. Scale bar represents 5 µm. **(C) Detection of MSH-5 foci at DSB repair sites in the absence of the SC-CR requires homolog engagement.** Top: Schematic of chromosome arrangements in early prophase in WT, (where all homologous chromosomes are paired and synapsed), in the *syp-1* mutant (in which homologs engage in strong pairwise associations in the vicinity of pairing centers (PC), but alignment is not stabilized by synapsis) and in the *him-8; syp-1* double mutant (in which the autosomes engage in unstable PC-mediated pairing, but the X chromosomes never pair). The autosomes are indicated in blue and red, the X chromosomes in red alone. HIM-8 is required for X chromosome pairing and synapsis. Bottom: representative images of early prophase spread nuclei from *syp-1* (top) and *him-8; syp-1* mutant gonads, probed for MSH-5, HTP-3, and di-methylated Lysine 4 on Histone 3 (H3K4me2), which specifically marks the autosomes, but not the X chromosomes. Multiple MSH-5 foci are detected on the X chromosomes in the *syp-1* single mutant, where the X chromosome are able to pair, but MSH-5 foci are absent from the unpaired X chromosomes in the *him-8; syp-1* double mutant. Scale bars represent 5 µm. **(D) ZHP-3 localizes to recombination sites lacking RPA in the SC-CR mutant.** Fields of nuclei from the early-to-late prophase transition regions of WT and *syp-1* spread gonads, probed for HTP-3 (red), BLM::HA (green), RPA-1 (blue) and ZHP-3, a conserved E3 ligase essential for crossing-over (red). Using spreading procedures, SC-associated ZHP-3 that is normally detected in whole-mount preparations of WT gonads is largely washed out, while recombination-site-associated ZHP-3 remains at sites lacking RPA. ZHP-3 is also detected at DNA repair sites in *syp-1* mutant gonads from the early-to-late-prophase transition onward, also at sites lacking RPA. Scale bar represents 5 µm.

STAR Methods

CONTACT FOR REAGENT AND RESOURCE SHARING

Supplement Figure 1

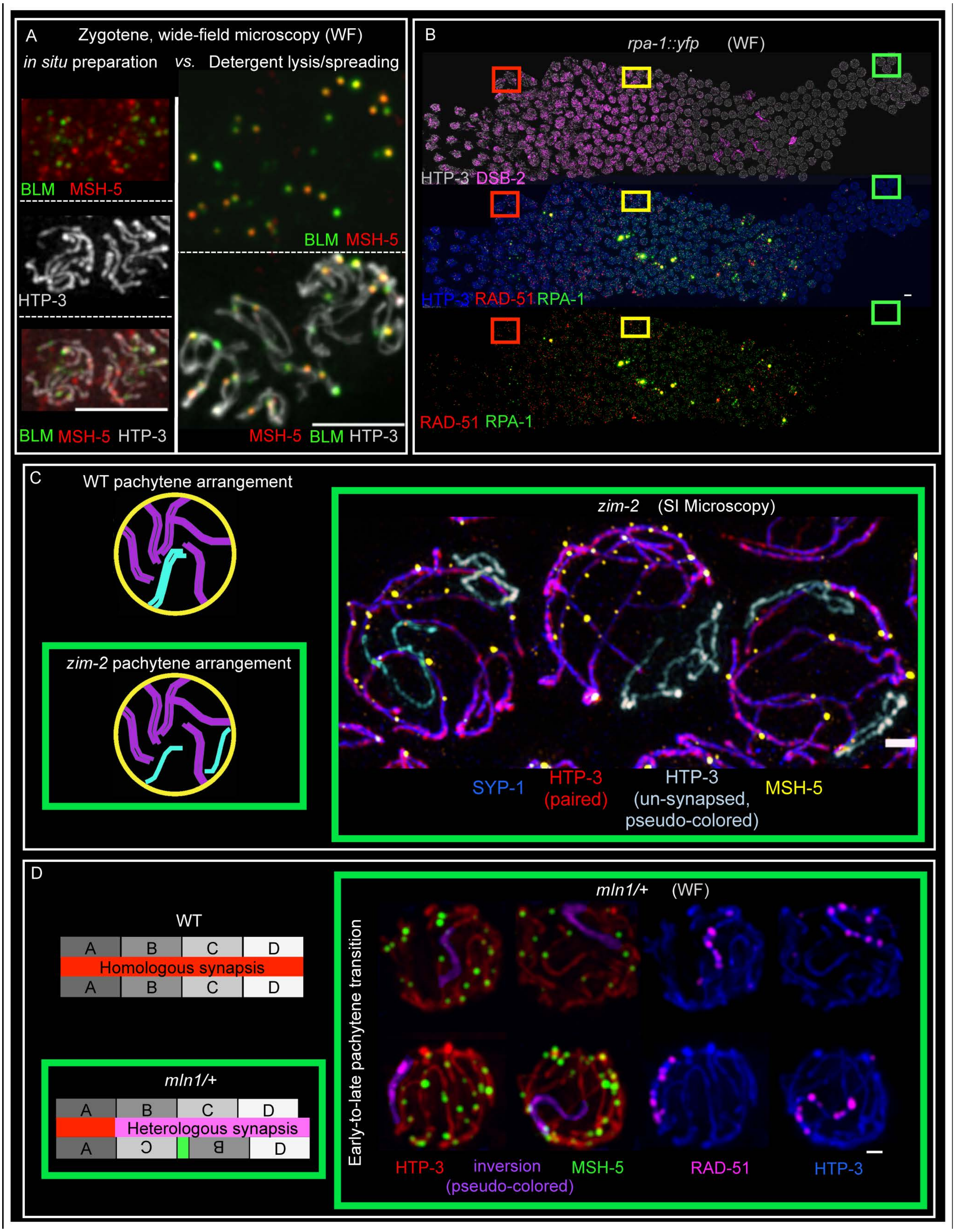

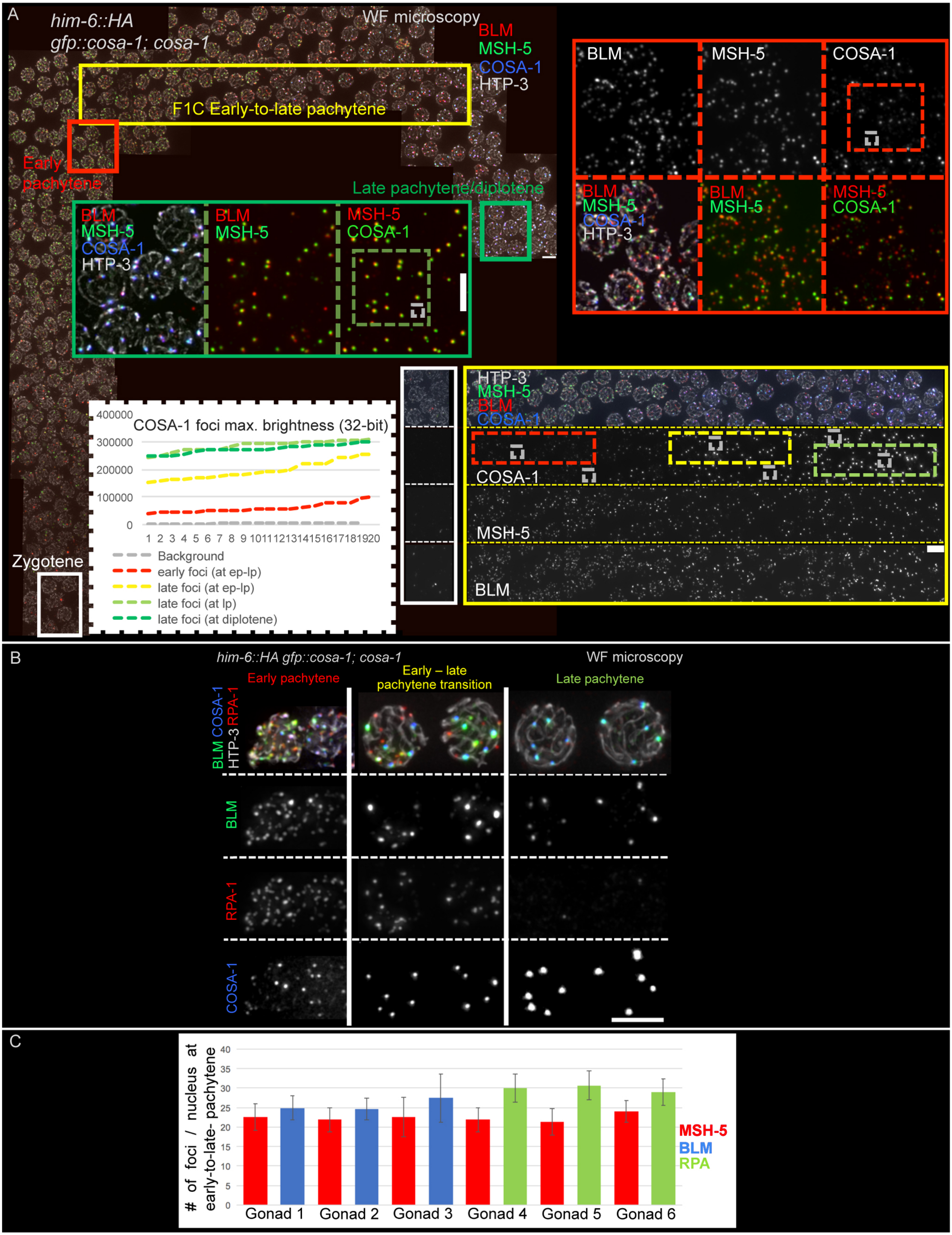
A
him-6::HA
gfp::cosa-1; cosa-1
WF microscopy
BLM
MSH-5
COSA-1
HTP-3
F1C Early-to-late pachytene
Early pachytene
Late pachytene/diplotene
Zygotene
BLM
MSH-5
COSA-1
HTP-3
BLM
MSH-5
MSH-5
COSA-1
BLM
MSH-5
COSA-1
BLM
MSH-5
COSA-1
HTP-3
BLM
MSH-5
MSH-5
COSA-1
COSA-1 foci max. brightness (32-bit)
400000
300000
200000
100000
0
1 2 3 4 5 6 7 8 9 10 11 12 13 14 15 16 17 18 19 20
Background
early foci (at ep-lp)
late foci (at ep-lp)
late foci (at lp)
late foci (at diplotene)
HTP-3
MSH-5
BLM
COSA-1
COSA-1
MSH-5
BLM
B
him-6::HA gfp::cosa-1; cosa-1
WF microscopy
Early pachytene
Early – late pachytene transition
Late pachytene
BLM COSA-1 RPA-1 HTP-3
BLM
RPA-1
COSA-1
C
# of foci / nucleus at early-to-late- pachytene
40
35
30
25
20
15
10
5
0
Gonad 1
Gonad 2
Gonad 3
Gonad 4
Gonad 5
Gonad 6
MSH-5
BLM
RPA

Supplement Figure 3

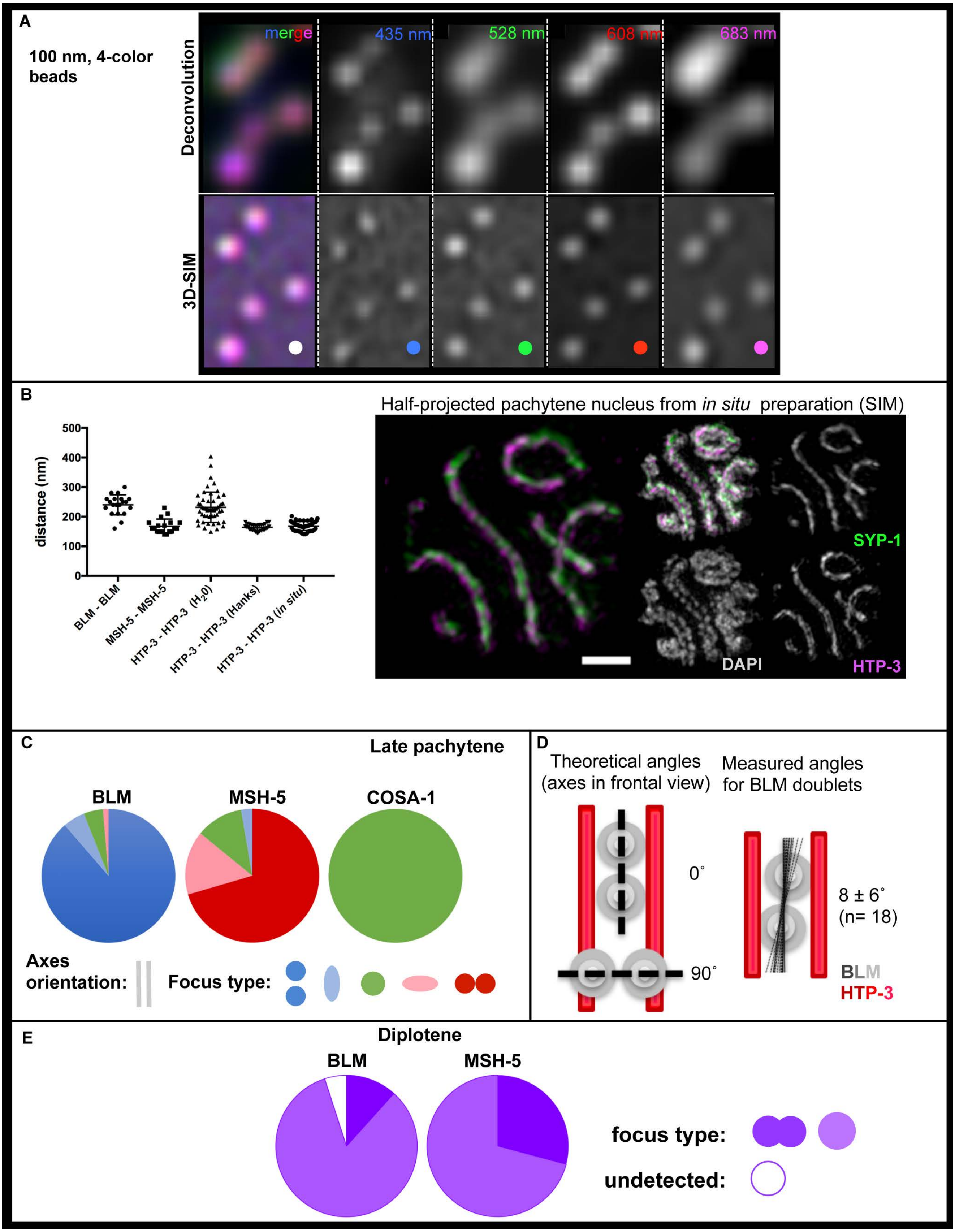

Supplement Figure 4

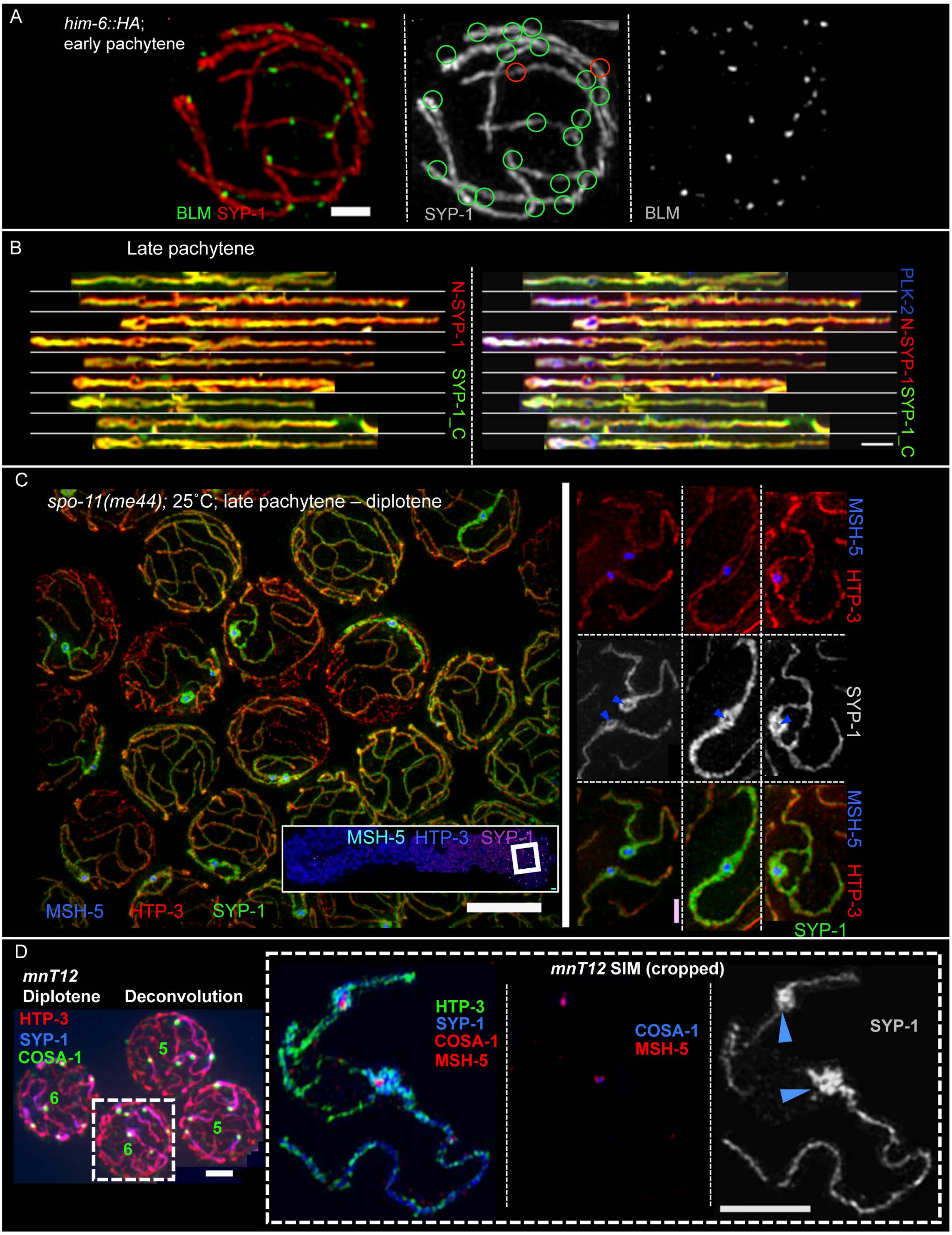

Supplement Figure 5